2023 62nd IEEE Conference on Decision and Control (CDC)
December 13-15, 2023. Marina Bay Sands, Singapore

Dynamical mode decomposition for infinite-dimensional open quantum systems; Liouvillian spectral analysis and parameter estimation

Yuzuru Kato and Hiroya Nakao

Abstract— Dynamic mode decomposition (DMD) is a data-driven method for the estimation, prediction, and control of complex dynamical systems, which has gained much attention in the fields of nonlinear dynamics and fluid mechanics. A DMD method for quantum spin systems, described by a linear dynamical system of a finite-dimensional set of observables, has been proposed recently. In this study, we propose two DMD methods applicable to infinite-dimensional open quantum systems, which use time-series data obtained by quantum state tomography. First, we propose a kernel DMD method for a data-driven spectral analysis of the Liouville superoperator. Second, we propose a method for the parameter estimation of the Liouville superoperator, which incorporates prior knowledge of the model structure into DMD. The proposed methods can accurately reconstruct the system dynamics and show that DMD frameworks can be applicable to infinite-dimensional open quantum systems.

I. Introduction

With the recent progress in quantum information science, the demand for reliable and consistent quantum control has been growing. The task of central importance for stable manipulation of quantum systems is to characterize the dynamics of black-box quantum systems from input-output data, and such a task is generally known as quantum process tomography [1], [2]. In the systems and control community, similar mathematical problems have been studied as quantum system identification [3], [4], and various methods for reconstructing the mathematical model of quantum system dynamics from input-output data have been proposed [3]–[12].

In the communities of nonlinear dynamics and fluid mechanics, dynamic mode decomposition (DMD) has gained much attention as a data-driven method for estimation, prediction, and control of complex dynamical systems [13]. Using DMD, we can approximately extract linearly evolving eigenmodes of complex nonlinear dynamical systems, e.g., oscillatory eigenmodes of a fluid system exhibiting Karman vortex streets, from time-series data. The original DMD is proposed by Schmid [14] for extracting spatiotemporal coherent structures in nonlinear complex fluid flows. Shortly after the original proposal, Rowley et. al. [15] clarified the relationship between DMD and Koopman operator theory for nonlinear dynamical systems [16], [17]. On the basis of this theoretical relationship, a large number of investigations have been carried out on DMD and its extensions such as Hankel DMD that uses time-delayed coordinates [18], [19], kernel DMD [20] and extended DMD [21] for efficient numerical computation, DMD with control [22], sparsity-promoting DMD [23], and DMD-based parameter estimation [24]–[26].

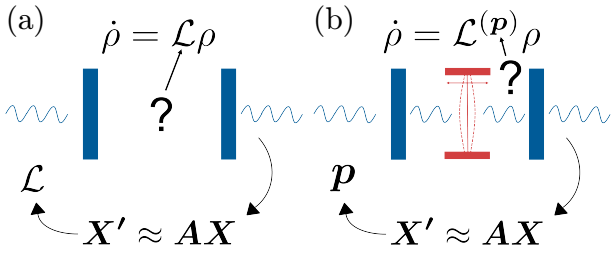

Fig. 1. Schematic diagram of DMD for infinite-dimensional open quantum systems. (a) Spectral analysis and (b) parameter estimation of the Liouville superoperator.

The DMD framework has also been applied to quantum systems recently. Goldschmidt proposed a bilinear DMD method for data-driven quantum control and numerically applied it to a single spin system [27], and we extended the applicability of DMD to quantum spin networks with limited access by using Hankel DMD [28]. Also, Klus applied DMD to quantum dynamical systems described by the Schrödinger equation [29], [30]. However, application of DMD to infinite-dimensional open quantum systems, which cannot be described by a finite-dimensional linear dynamical system, has not been studied.

In this study, we propose two DMD methods that are applicable to infinite-dimensional open quantum systems, which use the time-series data obtained by quantum state tomography [31], [32]. First, we propose a kernel DMD (KDMD) method, which approximately extracts the eigenvalues and eigenoperators of the Liouville superoperator from the time-series data. Second, we propose a DMD-based method for the parameter estimation of the Liouville superoperator, which provides better performance than the simple DMD by incorporating prior knowledge of the model structure into DMD. Figure 1 shows a schematic diagram of the two proposed methods. Using the quantum van der Pol oscillator with Kerr effect as an example, we numerically demonstrate

Yuzuru Kato is with the Department of Complex and Intelligent Systems, Future University Hakodate, Hokkaido 041-8655, Japan (email: katoyuzu@fun.ac.jp)

Hiroya Nakao is with the Department of Systems and Control Engineering, School of Engineering, Tokyo Institute of Technology, O-okayama 2-12-1, Meguro-ku, Tokyo, Japan (email: nakao@sc.e.titech.ac.jp)

that the proposed DMD methods can accurately reconstruct the system dynamics. Our results show that DMD frameworks can be applicable to infinite-dimensional open quantum systems.

This paper is organized as follows. In section II, we briefly review DMD, its numerical algorithm, and KDMD. In section III, we discuss KDMD for a data-driven spectral analysis of the Liouville superoperator. In section IV, we discuss a DMD-based parameter estimation method for the Liouville superoperator. Section V concludes the paper.

II. Overview of Dynamic mode decomposition

In this section, we provide a brief overview of DMD, its numerical algorithm with singular value decomposition (SVD) [13], [18], and KDMD that uses a kernel trick for reducing computational cost of DMD [20].

A. Dynamic mode decomposition

We consider a dynamical system

$$\frac{d\boldsymbol{x}}{dt} = \boldsymbol{F}(\boldsymbol{x}), \tag{1}$$

where $\boldsymbol{x} \in \mathbb{C}^N$ represents a system state and $\boldsymbol{F} : \mathbb{C}^N \to \mathbb{C}^N$ is a vector field representing the system dynamics. We collect time-series data $\{\boldsymbol{x}_k\}$ $(k = 1, 2, 3, \dots)$ from the system with a sampling interval of Δt, namely, $\boldsymbol{x}_k = \boldsymbol{x}(k\Delta t)$.

In DMD, using the collected time-series data, we seek a locally linear dynamical system approximating Eq. (1) as

$$\frac{d\boldsymbol{x}}{dt} \approx \mathcal{A}\boldsymbol{x}, \tag{2}$$

where $\mathcal{A} \in \mathbb{C}^{N\times N}$. The solution to Eq. (2) is written as

$$\boldsymbol{x}(t) = \sum_{j=1}^{N} \boldsymbol{\phi}_j \exp(\lambda_j t)\, b_j = \boldsymbol{\Phi} \exp(\boldsymbol{\lambda} t)\boldsymbol{b}, \tag{3}$$

where we introduced matrices $\boldsymbol{\Phi} = [\boldsymbol{\phi}_1, ..., \boldsymbol{\phi}_N]$, $\boldsymbol{\lambda} = \mathrm{diag}(\lambda_1, ..., \lambda_N)$ with diag representing a diagonal matrix, and a vector $\boldsymbol{b} = (b_1, ..., b_N)^{\mathsf{T}}$ with T representing the transpose. Here, $\{\lambda_j\}_{j=1}^N$ and $\{\boldsymbol{\phi}_j\}_{j=1}^N$ represent the eigenvalues and eigenvectors of the matrix $\mathcal{A}$, respectively, and $\{b_j\}_{j=1}^N$ represent the expansion coefficients (coordinates) of $\boldsymbol{x}(0)$ with respect to the eigenvector basis $\{\boldsymbol{\phi}_j\}_{j=1}^N$.

For this purpose, we construct two matrices $\boldsymbol{X}, \boldsymbol{X'} \in \mathbb{C}^{N\times(M-1)}$ using the time-series data $\{\boldsymbol{x}_k\}$ as

$$\boldsymbol{X} = \begin{bmatrix} \boldsymbol{x}_1 & \boldsymbol{x}_2 & \cdots & \boldsymbol{x}_{M-1} \end{bmatrix},\ \boldsymbol{X'} = \begin{bmatrix} \boldsymbol{x}_2 & \boldsymbol{x}_3 & \cdots & \boldsymbol{x}_M \end{bmatrix}. \tag{4}$$

Then, the local linear approximation can be written as

$$\boldsymbol{X'} \approx \boldsymbol{A}\boldsymbol{X},\ \ \boldsymbol{A} = \exp(\mathcal{A}\Delta t), \tag{5}$$

where $\boldsymbol{A} \in \mathbb{C}^{N\times N}$, and the optimal matrix $\boldsymbol{A}$ is obtained by solving

$$\boldsymbol{A} = \arg\min_{\bar{\boldsymbol{A}}} \left\| \boldsymbol{X'} - \bar{\boldsymbol{A}}\boldsymbol{X} \right\|_F, \tag{6}$$

where $\|\boldsymbol{C}\|_F = \sqrt{\sum_{j=1}^{N}\sum_{k=1}^{M-1} |C_{jk}|^2}$ represents the Frobenius norm of $\boldsymbol{C} \in \mathbb{R}^{N\times(M-1)}$. The solution to Eq. (6) is obtained as

$$\boldsymbol{A} = \boldsymbol{X'}\boldsymbol{X}^{+}, \tag{7}$$

where $+$ represents the Moore-Penrose pseudoinverse.

We can obtain Eq. (3) from the eigendecomposition of the matrix $\boldsymbol{A}$, where the eigenvalues λ_j of $\mathcal{A}$ are evaluated as $\lambda_j = \ln(\Lambda_j)/\Delta t$ from the eigenvalues Λ_j of $\boldsymbol{A}$ [13].

B. Numerical algorithm for DMD

In practice, when considering data matrices with large dimensions, the numerical calculation of the matrix $\boldsymbol{A}$ is time-consuming. In such cases, instead of $\boldsymbol{A}$, a rank-reduced SVD matrix $\tilde{\boldsymbol{A}}$ obtained by SVD of $\boldsymbol{X}$ is introduced. The numerical algorithm of DMD with SVD is performed as follows [13], [18].

1) We apply SVD to the original $\boldsymbol{X}$ and, by retaining only the dominant r singular values, obtain a rank-reduced matrix $\boldsymbol{X} \approx \boldsymbol{U}\boldsymbol{\Sigma}\boldsymbol{V}^{\dagger}$ with $\dagger$ representing the Hermitian conjugate (the same symbol $\boldsymbol{X}$ is used for the rank-reduced matrix), where $\boldsymbol{U} \in \mathbb{C}^{N\times r}, \boldsymbol{\Sigma} \in \mathbb{R}^{r\times r}, \boldsymbol{V} \in \mathbb{C}^{M\times r}$ (r is the rank of the reduced matrix), $\boldsymbol{U}^{\dagger}\boldsymbol{U} = \boldsymbol{I}^r, \boldsymbol{V}^{\dagger}\boldsymbol{V} = \boldsymbol{I}^r$, and $\boldsymbol{I}^k$ represents the k-dimensional identity matrix. The pseudoinverse of $\boldsymbol{X}$ can be approximately expressed as $\boldsymbol{X}^{+} \approx \boldsymbol{V}\boldsymbol{\Sigma}^{+}\boldsymbol{U}^{\dagger}$.
2) We construct a $r\times r$ matrix $\tilde{\boldsymbol{A}} = \boldsymbol{U}^{\dagger}(\boldsymbol{X'}\boldsymbol{V}\boldsymbol{\Sigma}^{+}\boldsymbol{U}^{\dagger})\boldsymbol{U} = \boldsymbol{U}^{\dagger}\boldsymbol{X'}\boldsymbol{V}\boldsymbol{\Sigma}^{+} \in \mathbb{C}^{r\times r}$, which is a projection of the matrix $\boldsymbol{A}$ onto the r SVD modes; that is, $\tilde{\boldsymbol{x}}_{k+1} = \tilde{\boldsymbol{A}}\tilde{\boldsymbol{x}}_k$ is approximately satisfied for the projected coordinate $\tilde{\boldsymbol{x}}_k = \boldsymbol{U}^{\dagger}\boldsymbol{x}_k$.
3) We take the eigendecomposition of $\tilde{\boldsymbol{A}}$ as $\tilde{\boldsymbol{A}}\boldsymbol{W} = \boldsymbol{W}\boldsymbol{\Lambda}$, where the columns of $\boldsymbol{W} \in \mathbb{C}^{r\times r}$ are the eigenvectors of $\tilde{\boldsymbol{A}}$ and $\boldsymbol{\Lambda} \in \mathbb{C}^{r\times r}$ is a diagonal matrix of the eigenvalues Λ_j $(j = 1, 2, \dots, r)$ of $\tilde{\boldsymbol{A}}$.
4) We approximately obtain the dominant r eigenvectors and eigenvalues of $\boldsymbol{A}$ as $\boldsymbol{\Phi} = \boldsymbol{X'}\boldsymbol{V}\boldsymbol{\Sigma}^{+}\boldsymbol{W} \in \mathbb{C}^{N\times r}$ and $\boldsymbol{\Lambda}$, respectively.

Using the obtained eigenvalues $\Lambda_1, ..., \Lambda_r$ and r-dimensional eigenvectors $\boldsymbol{\phi}_1, ..., \boldsymbol{\phi}_r$, we can approximately describe the state $\boldsymbol{x}(t)$ as

$$\boldsymbol{x}^d(t) \approx \sum_{j=1}^{r} \boldsymbol{\phi}_j^d \exp\left(\lambda_j^d t\right) b_j^d = \boldsymbol{\Phi}^d \exp(\boldsymbol{\lambda}^d t)\boldsymbol{b}^d, \tag{8}$$

where $\lambda_j^d = \ln(\Lambda_j^d)/\Delta t$. Setting the initial state at time $t = 0$ as $\boldsymbol{x}_1$, i.e., $\boldsymbol{x}_1 = \boldsymbol{x}^d(0) = \boldsymbol{\Phi}^d\boldsymbol{b}^d$, we obtain the coefficient vector $\boldsymbol{b}^d$ as $\boldsymbol{b}^d = (\boldsymbol{\Phi}^d)^{+}\boldsymbol{x}_1$.

C. Kernel DMD

The DMD algorithm in the last subsection requires the calculation of the pseudoinverse of $\boldsymbol{X}$, which is sometimes computationally expensive. We can incorporate the kernel trick with DMD for reducing the computational

cost when the dimension N of the system is much larger than the length M of the collected data, i.e., $N \gg M$ [13], [20].

We consider the eigenvalue problem $\Lambda_k \boldsymbol{\phi}_k = \boldsymbol{A}\boldsymbol{\phi}_k$ for the eigenvalue Λ_k and eigenvector $\boldsymbol{\phi}_k$ of $\boldsymbol{A}$. Introducing $\boldsymbol{\phi}_k = \boldsymbol{U}\tilde{\boldsymbol{\phi}}_k$, where $\tilde{\boldsymbol{\phi}}_k \in \mathbb{C}^{r\times 1}$, we approximately obtain

$$\begin{aligned}\Lambda_k \boldsymbol{U}\tilde{\boldsymbol{\phi}}_k &= \boldsymbol{A}\boldsymbol{U}\tilde{\boldsymbol{\phi}}_k = \boldsymbol{X}'\boldsymbol{X}^{+}\boldsymbol{U}\tilde{\boldsymbol{\phi}}_k = \boldsymbol{X}'\boldsymbol{X}^{+}\left(\boldsymbol{X}\boldsymbol{V}\boldsymbol{\Sigma}^{+}\right)\tilde{\boldsymbol{\phi}}_k \\ &= \boldsymbol{X}'\left(\boldsymbol{V}\boldsymbol{\Sigma}^{+}\right)\tilde{\boldsymbol{\phi}}_k = \left(\boldsymbol{X}^{\dagger}\right)^{+}\boldsymbol{X}^{\dagger}\boldsymbol{X}'\left(\boldsymbol{V}\boldsymbol{\Sigma}^{+}\right)\tilde{\boldsymbol{\phi}}_k \\ &= \left(\boldsymbol{X}^{\dagger}\right)^{+}\left(\boldsymbol{X}^{\dagger}\boldsymbol{X}'\right)\left(\boldsymbol{V}\boldsymbol{\Sigma}^{+}\right)\tilde{\boldsymbol{\phi}}_k \\ &= \boldsymbol{U}\left(\boldsymbol{\Sigma}^{+}\boldsymbol{V}^{\dagger}\right)\left(\boldsymbol{X}^{\dagger}\boldsymbol{X}'\right)\left(\boldsymbol{V}\boldsymbol{\Sigma}^{+}\right)\tilde{\boldsymbol{\phi}}_k = \boldsymbol{U}\tilde{\boldsymbol{A}}\tilde{\boldsymbol{\phi}}_k.\end{aligned} \tag{9}$$

Thus, the matrix $\tilde{\boldsymbol{A}}$ can be calculated in the KDMD algorithm by

$$\tilde{\boldsymbol{A}} = \left(\boldsymbol{\Sigma}^{+}\boldsymbol{V}^{\dagger}\right)\left(\boldsymbol{X}^{\dagger}\boldsymbol{X}'\right)\left(\boldsymbol{V}\boldsymbol{\Sigma}^{+}\right) \tag{10}$$

instead of 2) in the DMD algorithm. Here, $\left(\boldsymbol{\Sigma}^{+}\boldsymbol{V}^{\dagger}\right) \in \mathbb{C}^{r\times M}, \left(\boldsymbol{X}^{\dagger}\boldsymbol{X}'\right) \in \mathbb{C}^{M\times M}, \left(\boldsymbol{V}\boldsymbol{\Sigma}^{+}\right) \in \mathbb{C}^{M\times r}$ and $\boldsymbol{\Sigma}$, $\boldsymbol{V}$ are calculated by the eigendecomposition of the $M \times M$ matrix $\boldsymbol{V}\boldsymbol{\Sigma}^2 = \left(\boldsymbol{X}^{\dagger}\boldsymbol{X}\right)\boldsymbol{V}$. Therefore, the computational cost is determined by the length M of the collected data rather than the dimension N of the system, resulting in reduced computational cost when $N \gg M$.

In general, instead of using $\boldsymbol{X}$ and $\boldsymbol{X}'$, we introduce the set of feature vectors $\boldsymbol{\psi}(\boldsymbol{x}) = [\psi_1(\boldsymbol{x}), \psi_2(\boldsymbol{x}), \cdots, \psi_{N'}(\boldsymbol{x})]^{\mathsf{T}} \in \mathbb{C}^{N'\times 1}$ and use the data matrices $\boldsymbol{Y} = [\boldsymbol{\psi}(\boldsymbol{x}_1), \boldsymbol{\psi}(\boldsymbol{x}_2), \cdots, \boldsymbol{\psi}(\boldsymbol{x}_{M-1})]$, $\boldsymbol{Y}' = [\boldsymbol{\psi}(\boldsymbol{y}_1), \boldsymbol{\psi}(\boldsymbol{y}_2), \cdots, \boldsymbol{\psi}(\boldsymbol{y}_{M-1})]$, where $\boldsymbol{y}_k = \boldsymbol{F}(\boldsymbol{x}_k)$. In this setup, $\left(\boldsymbol{Y}^{\dagger}\boldsymbol{Y}'\right)$ can be calculated by using the kernel trick for the kernel function $f(\boldsymbol{x}, \boldsymbol{y}) = \boldsymbol{\psi}(\boldsymbol{x})^{\dagger}\boldsymbol{\psi}(\boldsymbol{y})$ defined from the set of chosen feature vectors $\boldsymbol{\psi}$.

III. Kernerl DMD for Liouvillian spectral analysis of oepn quantum systems

First, we propose KDMD for the spectral analysis of the Liouville superoperator for open quantum systems.

A. Open quantum systems

We consider general open quantum systems subjected to quantum dissipation arising from interactions with reservoirs, i.e., environmental quantum systems [33], [34]. Under the assumption that interactions of the system with the reservoirs are instantaneous and Markovian approximation can be employed, the time evolution of the system's density operator ρ is described by the quantum master equation

$$\dot{\rho} = \mathcal{L}\rho = -i[H, \rho] + \sum_{l=1}^{L} \mathcal{D}[C_l]\rho, \tag{11}$$

where $\mathcal{L}$ is a Liouville superoperator, H represents a system Hamiltonian, C_l represents a coupling operator between the system and lth reservoir ($l = 1, 2, \ldots, L$), $[A, B] = AB - BA$ represents the commutator, $\mathcal{D}[C]\rho = C\rho C^{\dagger} - (\rho C^{\dagger}C + C^{\dagger}C\rho)/2$ represents the Lindblad form, and the reduced Planck's constant is set as $\hbar = 1$.

We consider an infinite-dimensional open quantum system whose density operator is represented by the number-state basis, i.e., $\rho = \sum_{i,j} \rho_{ij}|i\rangle\langle j|$ ($i, j = 1, 2, \cdots$), such as quantum optical systems or quantum optomechanical systems. We can approximately describe the density operator ρ by a $n \times n$ density matrix ρ_n that is represented by the number-state basis up to n levels, by taking a sufficiently large number n with which ρ_n is trace preserving and positive with sufficient precision.

Then, the system dynamics is approximately described by

$$\dot{\rho_n} = \mathcal{L}_n\rho_n, \tag{12}$$

where $\mathcal{L}_n$ is the truncated Liouville superoperator $\mathcal{L}$ up to n levels. Using the transformation

$$A\rho_n B \leftrightarrow \left(A \otimes B^{\mathsf{T}}\right)|\rho_n\rangle\rangle, \tag{13}$$

the system dynamics in Eq. (12) is expressed in the vector representation as

$$\frac{d}{dt}|\rho_n\rangle\rangle = \boldsymbol{L}_n|\rho_n\rangle\rangle, \tag{14}$$

where $|\rho_n\rangle\rangle \in \mathbb{C}^{n^2\times 1}$ is a n^2-dimensional vector form of ρ_n and $\boldsymbol{L}_n$ is a representation of $\mathcal{L}_n$ by a $n^2 \times n^2$ matrix.

B. Kernerl DMD for Liouvillian spectral analysis

The DMD method can be used for a data-driven spectral analysis of the Liouvillie superoperator. We assume that we can collect time-series data $\boldsymbol{x}_k = |\rho_n(k\Delta t)\rangle\rangle$ of the system state via quantum state tomography (see Ref. [32] for an example of experimental setups). By performing DMD, we can reconstruct the matrix $\boldsymbol{A}$ in Eq. (5) as

$$\boldsymbol{X'} = \boldsymbol{A}\boldsymbol{X}, \ \boldsymbol{A} = \exp(\boldsymbol{L}_n\Delta t). \tag{15}$$

Therefore, we can perform an eigendecomposition of $\boldsymbol{L}_n$, where the eigenvalues of $\boldsymbol{L}_n$ are obtained as $\lambda_j = \ln(\Lambda_j)/\Delta t$ from the eigenvalues Λ_j of $\boldsymbol{A}$, and the eigenoperator U_j of $\mathcal{L}$ with the eigenvalue λ_j is approximately obtained from the eigenvector of $\boldsymbol{L}_n$.

Instead of DMD, we can also use KDMD for reducing the computational cost because, in quantum state tomography, the length M of the collected data needs to be small for reducing the number of experimental realizations whereas the dimension $N = n \times n$ of the sampled state sometimes becomes large, i.e., $N \gg M$. In this case, the kernel function $f(\boldsymbol{x}_k, \boldsymbol{x}_l) = \langle\langle\rho_n(k\Delta t)|\rho_n(l\Delta t)\rangle\rangle = \mathrm{Tr}\left[\rho_n(k\Delta t)\rho_n(l\Delta t)\right]$ defined from the feature vector $|\rho_n\rangle\rangle$ can be employed, which is a truncated version of the quantum kernel [35], [36], and the proposed KDMD method can be seen as a DMD method with reproducing kernels [37]. Though not discussed in this paper, it should be stressed that the proposed method can also be applied to finite-dimensional systems for which quantum state tomography can be performed, e.g., spins in silicon [38].

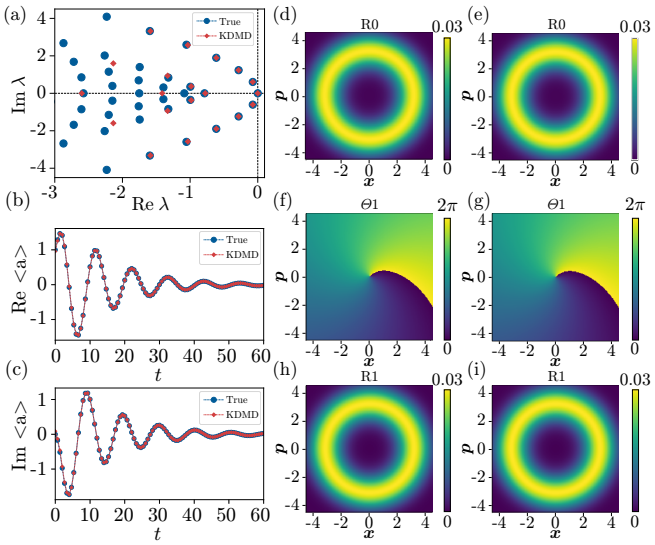

Fig. 2. Results of Kernel DMD for a quantum van der Pol oscillator with Kerr effect in the semiclassical regime. (a) Eigenvalues of $\mathcal{L}$ near the imaginary axis. (b,c) Time evolution of the mean value $\langle a \rangle$. (b) Re$\langle a \rangle$. (c) Im$\langle a \rangle$. (d, e) Eigenfunction R_0 for the zero eigenvalue λ_0. (f, g) Phase Θ_1 and (h, i) amplitude R_1 of the eigenfunction for the eigenvalue λ_1 with the smallest decay rate. (d, f, h) True eigenfunctions. (e, g, i) Reconstructed eigenfunctions. In (f), (g), $(x, p) = (\text{Re}\ \alpha, \text{Im}\ \alpha) = (2.296, 0)$ is chosen as the phase origin.

C. Numerical results

As an example, we consider a quantum van der Pol oscillator (also called quantum Stuart-landau oscillator [39] recently) with Kerr effect, which is a quantum nonlinear oscillator possessing a limit-cycle solution in the classical limit [40]–[42]. The system is described by a quantum master equation

$$\dot{\rho} = -i\,[H, \rho] + \gamma_1 \mathcal{D}[a^\dagger]\rho + \gamma_2 \mathcal{D}[a^2]\rho, \tag{16}$$

where a and $a^\dagger$ represent the annihilation and creation operators, $H = \omega_0 a^\dagger a + K a^{\dagger 2} a^2$ is the Hamiltonian, ω_0 represents the frequency parameter of the oscillator, K represents the Kerr parameter, and γ_1 and γ_2 represent the decay rates for negative damping and nonlinear damping, respectively. Note that this system cannot be described as a finite-dimensional linear dynamical quantum system [43].

First, we consider the semiclassical regime with parameters $(\omega_0, K, \gamma_1, \gamma_2) = (0.1, 0.025, 1, 0.05)$. We collected the time-series data of the sampled system with $n = 40$ $(N = 40^2 = 1600)$ levels for $M = 90$ time steps with the interval $\Delta = 2/3$ for $0 \le t \le 60$ from a pure initial coherent state $\rho = |\alpha_0\rangle\langle\alpha_0|$ with $\alpha_0 = 1$. We used $r = 20$ for the SVD calculation.

Figure 2(a) compares the true and reconstructed eigenvalues of the Liouvillie superoperator. It can be seen that more than 10 dominant eigenvalues are correctly reconstructed. Figures 2(b) and 2(c) compare the time evolution of the real and imaginary parts of the mean value $\langle a \rangle$, respectively, which are calculated from the true and reconstructed density operators. It can be seen that KDMD correctly reproduces the time evolution of these quantities. In Figs. 2(d-i), we compare the true and reconstructed eigenoperators. To evaluate the eigenoperator U_j, we use the quantity $u_j(\boldsymbol{\alpha}) = \langle \alpha | U_j | \alpha \rangle$, which is an eigenfunction of the time-shift operator in the P representation of the system [41], [42]. Figures 2(d, e) show $R_0 = u_0$ with the zero eigenvalue, $\lambda_0 = 0$, which corresponds to the steady-state of the system, and Figs. 2(f, g) and Figs. 2(h, i) show the phase $\Theta_1 = \arg u_1$ and amplitude $R_1 = |u_1|$ of the slowest eigenfunction u_1 for the eigenvalue $\lambda_1 = -\gamma_1 + i\Omega_1$ with the smallest decay rate γ_1 (we choose $\Omega_1 < 0$), respectively. It can be seen that these eigenoperators are also correctly reproduced by KDMD.

Next, we consider the strong quantum regime with parameters $(\omega_0, K, \gamma_1, \gamma_2) = (30, 10, 0.1, 0.4)$. We collected the time-series data of the sampled system with $n = 40$ $(N = 40^2 = 1600)$ for $M = 500$ steps with the interval $\Delta = 0.1$ for $0 \le t \le 50$ from a pure initial coherent state $\rho = |\alpha_0\rangle\langle\alpha_0|$ with $\alpha_0 = 1$. We used $r = 30$ for the SVD calculation.

Figure 3(a) shows the true and reconstructed eigenvalues of the Liouvillie superoperator. In the strong quantum regime, several dominant eigenmodes arise due to the strong Kerr effect. These eigenvalues are approximately given by $\widetilde{\lambda}_m = i[-\omega_0 - 2(m-1)K] - \frac{1}{2}\{\gamma_1(2m+1) + 2\gamma_2(m-1)^2$ $(m = 1, 2, \ldots)$ [40]–[42], which are indicated by the dotted lines in Fig. 3(a). As can be seen in the figure, KDMD can correctly reproduce the eigenvalues of the zero and the slowest eigenmodes, but it cannot reproduce the other dominant eigenvalues. Figures 3(b) and 3(c) show the time evolution of the mean values Re $\langle a \rangle$ and Im $\langle a \rangle$, respectively. Although the KDMD correctly reproduces the collected time-series data, the linearly interpolated data points show a zigzag time evolution. This is because the quick rotating motion arising from several dominant eigenmodes associated with eigenvalues with large imaginary parts cannot be captured with the large sampling interval used here; it is also the reason for the failure of capturing several dominant eigenvalues in Fig. 3(a). This problem may be solved by collecting data with a smaller sampling interval, but it requires a larger number of experimental realizations in the data collection as we need the entire time series until the system converges to the steady state for reconstructing the other eigenmodes accurately.

Figures 3(d-i) compare the true and reconstructed eigenoperators, where R_0, Φ_1, and R_1 are shown in Figs. 3(d-e), Figs. 3(f-g), and Figs. 3(h-i), respectively. We can see that these eigenoperators are correctly reconstructed.

IV. DMD for Liouvillian parameter estimation for open quantum systems

KDMD used in the previous section is a model-free method and does not require prior knowledge of the

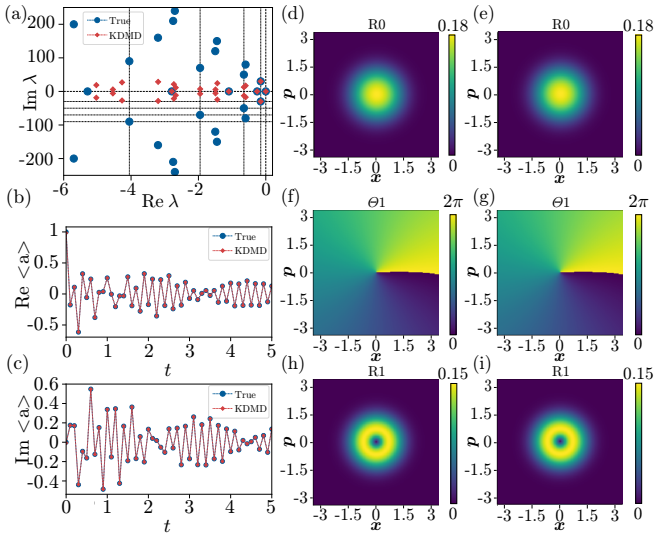

Fig. 3. Results of Kernel DMD for a quantum van der Pol oscillator with Kerr effect in the strong quantum regime. (a) Eigenvalues of $\mathcal{L}$ near the imaginary axis. (b,c) Time evolution of the mean value $\langle a \rangle$. (b) Re$\langle a \rangle$. (c) Im$\langle a \rangle$. (d, e) Eigenfunction R_0 for the zero eigenvalue λ_0. (f, g) Phase Θ_1 and (h, i) amplitude R_1 of the eigenfunction for the eigenvalue λ_1 with the smallest decay rate. (d, f, h) True eigenfunctions. (e, g, i) Reconstructed eigenfunctions. In (f), (g), $(x, p) = (\mathrm{Re}\ \alpha, \mathrm{Im}\ \alpha) = (1.786, 0)$ is chosen as the phase origin.

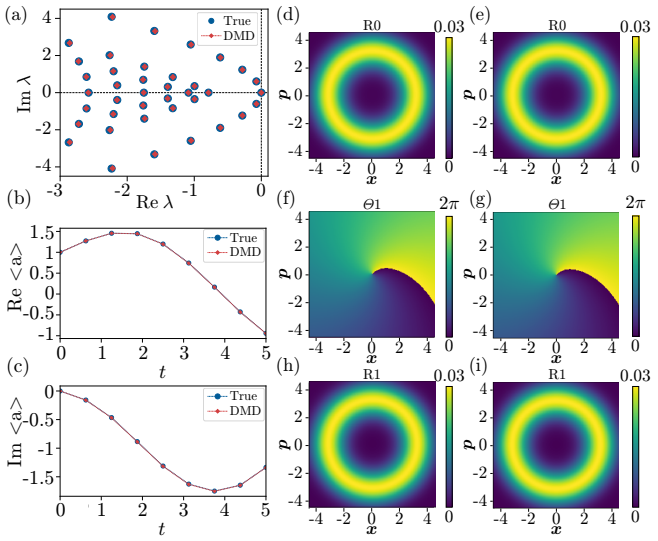

Fig. 4. Results of DMD-based parameter estimation for a quantum van der Pol oscillator with Kerr effect in the semiclassical regime. (a) Eigenvalues of $\mathcal{L}$ near the imaginary axis. (b,c) Time evolution of the mean value $\langle a \rangle$. (b) Re$\langle a \rangle$. (c) Im$\langle a \rangle$. (d, e) Eigenfunction R_0 for the zero eigenvalue λ_0. (f, g) Phase Θ_1 and (h, i) amplitude R_1 of the eigenfunction for the eigenvalue λ_1 with the smallest decay rate. (d, f, h) True eigenfunctions. (e, g, i) Reconstructed eigenfunctions. In (f), (g), $(x, p) = (\mathrm{Re}\ \alpha, \mathrm{Im}\ \alpha) = (2.296, 0)$ is chosen as the phase origin. Figures 4(d,f,h) are the same as Figs. 2(d,f,h).

model structure of the system dynamics. In quantum systems, we sometimes consider the cases where the model structure of the system dynamics is known and only its parameters are unknown, e.g., in considering experimental setups of quantum optical systems. In this section, we propose a method for estimating the parameters of the Liouvillie superoperator that incorporates the prior knowledge of the model structure into DMD.

A. Open quantum system with unknown parameters

We consider an open quantum system described by

$$\dot{\rho} = \mathcal{L}^{(\boldsymbol{p})}\rho, \tag{17}$$

where the structure of the Liouvillie superoperator $\mathcal{L}^{(\boldsymbol{p})}$ is known, but its parameters $\boldsymbol{p} = \{p_1, p_2, \ldots\}$ are unknown.

As in the previous section, we consider an infinite-dimensional open quantum system whose density operator is represented in the number-state basis. Taking a sufficiently large number n, we can approximately describe the density operator ρ by a $n \times n$ density matrix ρ_n with respect to the number-state basis up to n levels.

The system dynamics are then approximately described by

$$\dot{\rho_n} = \mathcal{L}_n^{(\boldsymbol{p})}\rho_n, \tag{18}$$

where $\mathcal{L}_n^{(\boldsymbol{p})}$ is the truncation of the Liouville superoperator $\mathcal{L}^{(\boldsymbol{p})}$ up to n levels. Using the transformation in Eq. (13), the system dynamics in Eq. (18) is reformulated in the vector representation

$$\frac{d}{dt}|\rho_n\rangle\rangle = \boldsymbol{L}_n^{(\boldsymbol{p})}|\rho_n\rangle\rangle, \tag{19}$$

where $\boldsymbol{L}_n^{(\boldsymbol{p})}$ is the $n^2 \times n^2$ dimensional matrix representation of $\mathcal{L}_n^{(\boldsymbol{p})}$.

B. DMD for Liouvillian parameter estimation

As in the previous section, we assume that we collect the time-series data $\boldsymbol{x}_k = |\rho_n(k\Delta t)\rangle\rangle$ of the system via quantum state tomography. When performing DMD, we reconstruct the matrix $\boldsymbol{A}$ in Eq. (5) as

$$\boldsymbol{X'} = \boldsymbol{A}\boldsymbol{X}, \ \ \boldsymbol{A} = \exp(\boldsymbol{L}_n^{(\boldsymbol{p})}\Delta t). \tag{20}$$

Further, projecting $\boldsymbol{X}$ on the r SVD modes gives

$$\tilde{\boldsymbol{X}}' = \tilde{\boldsymbol{A}}\tilde{\boldsymbol{X}}, \ \ \tilde{\boldsymbol{A}} = \exp(\tilde{\boldsymbol{L}}_n^{(\boldsymbol{p})}\Delta t), \tag{21}$$

where $\tilde{\boldsymbol{X}}' = \boldsymbol{U}^\dagger\boldsymbol{X}'$, $\tilde{\boldsymbol{X}} = \boldsymbol{U}^\dagger\boldsymbol{X}$, and $\tilde{\boldsymbol{L}}_n^{(\boldsymbol{p})} = \boldsymbol{U}^\dagger\boldsymbol{L}_n^{(\boldsymbol{p})}\boldsymbol{U}$.

This indicates that the unknown parameters $\boldsymbol{p}$ can be estimated by solving the following optimization problem:

$$\boldsymbol{p}_{est} = \arg\min_{\boldsymbol{p}} \left\| \tilde{\boldsymbol{X}}' - \exp(\tilde{\boldsymbol{L}}_n^{(\boldsymbol{p})}\Delta t)\tilde{\boldsymbol{X}} \right\|_F. \tag{22}$$

Using the estimated parameters $\boldsymbol{p}_{est}$, we can also reconstruct the Liouvillie superoperator as $\mathcal{L}^{(\boldsymbol{p}_{est})}$.

It should be noted that the proposed method can be seen as a counterpart of the DMD-based method for the Fokker-Planck operator of stochastic dynamical systems [24].

In this study, we use the scipy.optimize.minimize toolbox with the Limited-memory BFGS-B (L-BFGS-B) method for Python [44] to solve the optimization problem in Eq. (22). As the problem is non-convex, we

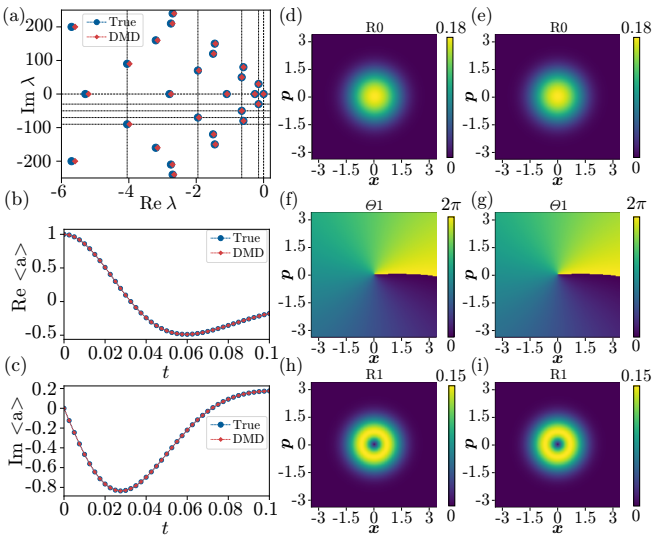

Fig. 5. Results of the DMD-based parameter estimation for a quantum van der Pol oscillator with Kerr effect in the strong quantum regime. (a) Eigenvalues of $\mathcal{L}$ near the imaginary axis. (b,c) Time evolution of the mean value $\langle a\rangle$. (b) Re$\langle a\rangle$. (c) Im$\langle a\rangle$. (d, e) Eigenfunction R_0 for the zero eigenvalue λ_0. (f, g) Phase Θ_1 and (h, i) amplitude R_1 of the eigenfunction for the eigenvalue λ_1 with the smallest decay rate. (d, f, h) True eigenfunctions. (e, g, i) Reconstructed eigenfunctions. In (f), (g), $(x, p) = (\mathrm{Re}\ \alpha, \mathrm{Im}\ \alpha) = (1.786, 0)$ is chosen as the phase origin. Figures 5(d,f,h) are the same as Figs. 3(d,f,h).

need to use multiple initial guesses to find the optimal solution.

C. Numerical results

As an example, we consider a quantum van der Pol oscillator with Kerr effect described by the quantum master equation (16) whose parameters $\boldsymbol{p} = (\omega_0, K, \gamma_1, \gamma_2)$ are unknown. In numerical simulations, we set the range of the parameters as $\omega_0 \in [-\infty, \infty], K, \gamma_1, \gamma_2 \in [0, \infty]$.

First, we consider the semiclassical regime with the parameters $(\omega_0, K, \gamma_1, \gamma_2) = (0.1, 0.025, 1, 0.05)$. We collected the time-series data of the sampled system with $n = 40$ $(N = 40^2 = 1600)$ for $M = 8$ steps with the interval $\Delta = 5/8$ for $0 \le t \le 5$ from a pure initial coherent state $\rho = |\alpha_0\rangle\langle\alpha_0|$ with $\alpha_0 = 1$. We used $r = M = 8$ for the SVD calculation.

Solving the optimization problem in Eq. (22), we estimated the parameters as $\boldsymbol{p}_{est} = (0.103, 0.0248, 1.001, 0.0501)$, which are sufficiently accurate, and reconstructed the Liouvillie superoperator as $\mathcal{L}^{(\boldsymbol{p}_{est})}$.

Figure 4(a) shows the eigenvalues of the true and reconstructed Liouvillie superoperator. It can be seen that all eigenvalues are correctly reproduced. Figures 4(b) and 4(c) show the time evolution of the mean values Re $\langle a\rangle$ and Im $\langle a\rangle$, respectively. It can be seen that the time evolution of these quantities are also correctly reproduced.

Figures 4(d-i) compare the true and reconstructed eigenoperators, where R_0, Φ_1, and R_1 are shown in Figs. 4(d-e), Figs. 4(f-g), and Figs. 4(h-i), respectively. We can see that these eigenoperators are correctly reconstructed. Here, it is remarkable that we need only $M = 8$ time steps of the collected data for estimating the parameters correctly.

Next, we consider the strong quantum regime with the parameters $(\omega_0, K, \gamma_1, \gamma_2) = (30, 10, 0.1, 0.4)$. We collected the time-series data of the sampled system with $n = 40$ $(N = 40^2 = 1600)$ for $M = 40$ steps with the interval $\Delta = 1/400$ for $0 \le t \le 0.1$ from a pure initial coherent state $\rho = |\alpha_0\rangle\langle\alpha_0|$ with $\alpha_0 = 1$. We used $r = M = 40$ for the SVD calculation.

Solving the optimization problem in Eq. (22), we could accurately estimate the parameters as $\boldsymbol{p}_{est} = (30.0, 10.0, 0.101, 0.391)$ and reconstruct the Liouvillie superoperator as $\mathcal{L}^{(\boldsymbol{p}_{est})}$.

Figure 5(a) shows the eigenvalues of the true and reconstructed Liouvillie superoperator. It can be seen that all eigenvalues, including the several dominant eigenvalues indicated by the dotted lines, are accurately reproduced. Figures 5(b) and 5(c) show the time evolution of the mean values Re $\langle a\rangle$ and Im $\langle a\rangle$, respectively. The time evolution of these quantities are also correctly reproduced.

Figures 5(d-i) compare the true and reconstructed eigenoperators, where R_0, Φ_1, and R_1 are shown in Figs. 5(d-e), Figs. 5(f-g), and Figs. 5(h-i), respectively. We can confirm that these eigenoperators are correctly reconstructed.

In the present parameter estimation, we can also reconstruct the adjoint Liouvillie superoperator $\mathcal{L}^*$ with respect to an inner product $\langle X, Y\rangle_{tr} = \mathrm{Tr}\,[X^\dagger Y]$ for linear operators X and Y, i.e., $\langle \mathcal{L}^* X, Y\rangle_{tr} = \langle X, \mathcal{L}Y\rangle_{tr}$, by using the estimated parameter as $(\mathcal{L}^{(\boldsymbol{p}_{est})})^*$. Since the adjoint Liouvillie superoperator $\mathcal{L}^*$ corresponds to the infinitesimal generator of the Koopman operator for open quantum systems [41], [42], the eigenoprator V_j with the eigenvalue λ_j corresponds to the jth Koopman eigenfunction of the system.

Figure 6 compares $\Phi_m(\boldsymbol{\alpha}) = \arg\langle\alpha|V_m|\alpha\rangle$ obtained from the true adjoint Liouvillie superoperator $\mathcal{L}^*$ with those obtained from the reconstructed adjoint operator $(\mathcal{L}^{(\boldsymbol{p}_{est})})^*$ for dominant eigenvalues $\widetilde{\lambda}_m$ $(m = 1, 2, 3, 4)$; these quantities characterize the quantum asymptotic phases of a quantum nonlinear oscillator [41], [42]. We can confirm that the asymptotic phases are correctly reconstructed by the present method.

V. Conclusion

We proposed two DMD methods applicable to infinite-dimensional open quantum systems; a KDMD method for data-driven spectral analysis and a DMD-based parameter estimation method for the Liouville superoperator.

In this study, we only consider an example of a quantum nonlinear oscillator. In future works, it is important

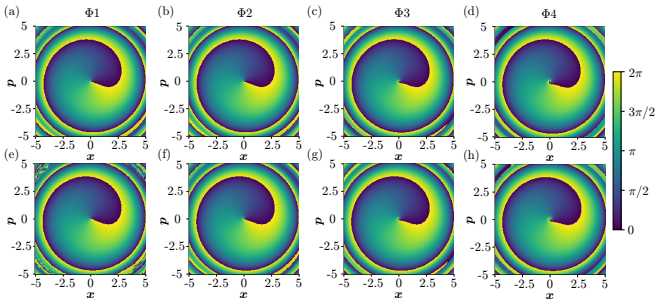

Fig. 6. Quantum asymptotic phases of the quantum van der Pol oscillator with Kerr effect in the strong quantum regime. (a, e) Φ_1, (b, f) Φ_2, (c, g) Φ_3, and (d, h) Φ_4. (a, b, c, d) True functions. (e,f,g,h) Reconstructed functions. In all figures, $(x, p) = (\mathrm{Re}\,\alpha, \mathrm{Im}\,\alpha) = (2.5, 0)$ is chosen as the phase origin where $\Phi_m = 0$ $(m = 1, 2, 3, 4)$.

to discuss the applicability of the proposed methods to more complex quantum networked systems. Compared to the other system identification methods, the proposed methods are expected to produce a better performance when the system exhibits coherent dynamics and is approximately described by a few dominant variables. However, even in such cases, the dimensionality of the system can still become large, and reducing the computational cost of the proposed methods is a future work.

We can also apply the proposed methods to finite-dimensional quantum spin systems for which quantum process tomography can be performed [38]. We can also formulate a DMD framework and compare with the other system identification methods for finite-dimensional linear dynamical quantum systems [43].

It is also interesting to discuss the data-driven reconstruction of decoherence-free subspaces [45], [46] by using DMD [28], which may also be used in the time-series analysis of electromagnetically induced transparency (EIT) [47], [48] for designing dark states of the quantum system. It is also important to discuss the effect of noisy measurement on the proposed methods [8], [9].

Other variants of the DMD method can also be applied for quantum system identification. For example, it would also be possible to extend the proposed DMD methods to include control input [22] in a similar manner to the bilinear DMD [27] and model predictive control [49] for quantum spin systems, which may be useful for data-driven quantum control of infinite-dimensional open quantum systems.

The DMD is a useful framework for data-driven estimation, prediction, and control of nonlinear complex dynamical systems [13]. The DMD framework may play important roles in analyzing and controlling complex nonlinear quantum many-body systems in the growing field of quantum science and technology.

VI. Acknowledgments

We acknowledge JSPS KAKENHI JP20J13778, JP22K14274, JP22K11919, JP22H00516 and JST CREST JP-MJCR1913 for financial support.

References

[1] I. L. Chuang and M. A. Nielsen, "Prescription for experimental determination of the dynamics of a quantum black box," Journal of Modern Optics, vol. 44, no. 11-12, pp. 2455–2467, 1997.
[2] M. Mohseni, A. Rezakhani, and D. Lidar, "Quantum-process tomography: Resource analysis of different strategies," Physical Review A, vol. 77, no. 3, p. 032322, 2008.
[3] D. Burgarth and K. Yuasa, "Quantum system identification," Physical Review Letters, vol. 108, no. 8, p. 080502, 2012.
[4] S. G. Schirmer, D. K. Oi, W. Zhou, E. Gong, and M. Zhang, "Open quantum system identification," arXiv preprint arXiv:1205.6220, 2012.
[5] H. Mabuchi, "Dynamical identification of open quantum systems," Quantum and Semiclassical Optics: Journal of the European Optical Society Part B, vol. 8, no. 6, p. 1103, 1996.
[6] D. Burgarth, K. Maruyama, and F. Nori, "Coupling strength estimation for spin chains despite restricted access," Physical Review A, vol. 79, no. 2, p. 020305, 2009.
[7] Y. Kato and N. Yamamoto, "Structure identification and state initialization of spin networks with limited access," New Journal of Physics, vol. 16, no. 2, p. 023024, 2014.
[8] J. Zhang and M. Sarovar, "Quantum Hamiltonian identification from measurement time traces," Physical Review Letters, vol. 113, no. 8, p. 080401, 2014.
[9] J. Zhang and M. Sarovar, "Identification of open quantum systems from observable time traces," Physical Review A, vol. 91, no. 5, p. 052121, 2015.
[10] S.-Y. Hou, H. Li, and G.-L. Long, "Experimental quantum Hamiltonian identification from measurement time traces," Science Bulletin, vol. 62, no. 12, pp. 863–868, 2017.
[11] H. I. Nurdin, N. H. Amini, and J. Chen, "Data-driven system identification of linear quantum systems coupled to time-varying coherent inputs," in 2020 59th IEEE Conference on Decision and Control (CDC). IEEE, 2020, pp. 3829–3835.
[12] M. Guţă and N. Yamamoto, "System identification for passive linear quantum systems," IEEE Transactions on Automatic Control, vol. 61, no. 4, pp. 921–936, 2015.
[13] J. N. Kutz, S. L. Brunton, B. W. Brunton, and J. L. Proctor, Dynamic mode decomposition: data-driven modeling of complex systems. SIAM, 2016.
[14] P. J. Schmid, "Dynamic mode decomposition of numerical and experimental data," Journal of Fluid Mechanics, vol. 656, pp. 5–28, 2010.
[15] C. W. Rowley, I. Mezić, S. Bagheri, P. Schlatter, and D. Henningson, "Spectral analysis of nonlinear flows," Journal of Fluid Mechanics, vol. 641, no. 1, pp. 115–127, 2009.
[16] I. Mezić, "Spectral properties of dynamical systems, model reduction and decompositions," Nonlinear Dynamics, vol. 41, no. 1-3, pp. 309–325, 2005.
[17] I. Mezić, "Analysis of fluid flows via spectral properties of the Koopman operator," Annual Review of Fluid Mechanics, vol. 45, pp. 357–378, 2013.
[18] J. H. Tu, C. W. Rowley, D. M. Luchtenburg, S. L. Brunton, and J. N. Kutz, "On dynamic mode decomposition: Theory and applications," Journal of Computational Dynamics, vol. 1, no. 2, p. 391, 2014.
[19] H. Arbabi and I. Mezic, "Ergodic theory, dynamic mode decomposition, and computation of spectral properties of the Koopman operator," SIAM Journal on Applied Dynamical Systems, vol. 16, no. 4, pp. 2096–2126, 2017.
[20] M. O. Williams, C. W. Rowley, and I. G. Kevrekidis, "A kernel-based approach to data-driven Koopman spectral analysis," arXiv preprint arXiv:1411.2260, 2014.
[21] M. O. Williams, I. G. Kevrekidis, and C. W. Rowley, "A data–driven approximation of the Koopman operator: Extending dynamic mode decomposition," Journal of Nonlinear Science, vol. 25, no. 6, pp. 1307–1346, 2015.

[22] J. L. Proctor, S. L. Brunton, and J. N. Kutz, "Dynamic mode decomposition with control," SIAM Journal on Applied Dynamical Systems, vol. 15, no. 1, pp. 142–161, 2016.
[23] M. R. Jovanović, P. J. Schmid, and J. W. Nichols, "Sparsity-promoting dynamic mode decomposition," Physics of Fluids, vol. 26, no. 2, p. 024103, 2014.
[24] A. N. Riseth and J. P. Taylor-King, "Operator fitting for parameter estimation of stochastic differential equations," arXiv preprint arXiv:1709.05153, 2017.
[25] A. Mauroy and J. Goncalves, "Koopman-based lifting techniques for nonlinear systems identification," IEEE Transactions on Automatic Control, vol. 65, no. 6, pp. 2550–2565, 2019.
[26] A. Mauroy, "Koopman operator framework for spectral analysis and identification of infinite-dimensional systems," Mathematics, vol. 9, no. 19, p. 2495, 2021.
[27] A. Goldschmidt, E. Kaiser, J. L. Dubois, S. L. Brunton, and J. N. Kutz, "Bilinear dynamic mode decomposition for quantum control," New Journal of Physics, vol. 23, no. 3, p. 033035, 2021.
[28] Y. Kato and H. Nakao, "Data-driven spectral analysis of quantum spin networks with limited access using Hankel dynamic mode decomposition," in 2022 IEEE 61st Conference on Decision and Control (CDC). IEEE, 2022, pp. 5141–5148.
[29] S. Klus, F. Nüske, and B. Hamzi, "Kernel-based approximation of the koopman generator and schrödinger operator," Entropy, vol. 22, no. 7, p. 722, 2020.
[30] S. Klus, F. Nüske, and S. Peitz, "Koopman analysis of quantum systems," arXiv preprint arXiv:2201.12062, 2022.
[31] W. P. Schleich, Quantum optics in phase space. John Wiley & Sons, 2011.
[32] S. Deleglise, I. Dotsenko, C. Sayrin, J. Bernu, M. Brune, J.-M. Raimond, and S. Haroche, "Reconstruction of non-classical cavity field states with snapshots of their decoherence," Nature, vol. 455, no. 7212, pp. 510–514, 2008.
[33] H.-P. Breuer, F. Petruccione et al., The theory of open quantum systems. Oxford University Press on Demand, 2002.
[34] H. J. Carmichael, Statistical Methods in Quantum Optics 1, 2. New York: Springer, 2007.
[35] M. Schuld and N. Killoran, "Quantum machine learning in feature hilbert spaces," Physical Review Letters, vol. 122, no. 4, p. 040504, 2019.
[36] M. Schuld, "Supervised quantum machine learning models are kernel methods," arXiv preprint arXiv:2101.11020, 2021.
[37] Y. Kawahara, "Dynamic mode decomposition with reproducing kernels for Koopman spectral analysis," in Proceedings of the 30th International Conference on Neural Information Processing Systems, 2016, pp. 919–927.
[38] K. Takeda, A. Noiri, T. Nakajima, J. Yoneda, T. Kobayashi, and S. Tarucha, "Quantum tomography of an entangled three-qubit state in silicon," Nature Nanotechnology, vol. 16, no. 9, pp. 965–969, 2021.
[39] A. Chia, L. Kwek, and C. Noh, "Relaxation oscillations and frequency entrainment in quantum mechanics," Physical Review E, vol. 102, no. 4, p. 042213, 2020.
[40] N. Lörch, E. Amitai, A. Nunnenkamp, and C. Bruder, "Genuine quantum signatures in synchronization of anharmonic self-oscillators," Physical Review Letters, vol. 117, no. 7, p. 073601, 2016.
[41] Y. Kato and H. Nakao, "A definition of the asymptotic phase for quantum nonlinear oscillators from the Koopman operator viewpoint," Chaos: An Interdisciplinary Journal of Nonlinear Science, vol. 32, no. 6, p. 063133, 2022.
[42] Y. Kato and H. Nakao, "Quantum asymptotic phases reveal signatures of quantum synchronization," New Journal of Physics, vol. 25, no. 2, p. 023012, 2023.
[43] H. I. Nurdin and N. Yamamoto, "Linear dynamical quantum systems," in Analysis, Synthesis, and Control. Springer, 2017.
[44] P. Virtanen, R. Gommers, T. E. Oliphant, M. Haberland, T. Reddy, D. Cournapeau, E. Burovski, P. Peterson, W. Weckesser, J. Bright et al., "Scipy 1.0: fundamental algorithms for scientific computing in python," Nature Methods, vol. 17, no. 3, pp. 261–272, 2020.
[45] D. A. Lidar, I. L. Chuang, and K. B. Whaley, "Decoherence-free subspaces for quantum computation," Physical Review Letters, vol. 81, no. 12, p. 2594, 1998.
[46] D. A. Lidar and K. B. Whaley, "Decoherence-free subspaces and subsystems," in Irreversible quantum dynamics. Springer, 2003, pp. 83–120.
[47] O. Kocharovskaya, "Coherent amplification of an ultrashort pulse in a three-level medium without a population inversion," Pis' ma Zh. Eksp. Teor. Fiz., vol. 48, pp. 581–584, 1988.
[48] S. E. Harris, "Lasers without inversion: Interference of lifetime-broadened resonances," Physical Review Letters, vol. 62, no. 9, p. 1033, 1989.
[49] A. J. Goldschmidt, J. L. DuBois, S. L. Brunton, and J. N. Kutz, "Model predictive control for robust quantum state preparation," arXiv preprint arXiv:2201.05266, 2022.